Available online at www.sciencedirect.com
SCIENCE DIRECT
Acta Materialia 54 (2006) 587–599
Acta MATERIALIA
www.actamat-journals.com

# Pseudoelasticity in Co–Ni–Al single and polycrystals

R.F. Hamilton [a], H. Sehitoglu [a,*], C. Efstathiou [a], H.J. Maier [b], Y. Chumlyakov [c]

[a] University of Illinois, Department of Mechanical and Industrial Engineering, 1206 W. Green St., Urbana, IL 61801, USA
[b] University of Paderborn, Lehrstuhl f. Werkstoffkunde, D-33095 Paderborn, Germany
[c] Siberian Physical Technical Institute, Revolution Sq. 1, Tomsk 634050, Russia

Received 16 May 2005; received in revised form 20 September 2005; accepted 21 September 2005
Available online 22 November 2005

**Abstract**

The pseudoelastic responses of heat-treated CoNiAl single crystals with [0 0 1] and [1 1 5] orientations, multicrystals of nominally [1 2 3] orientation, and polycrystals are investigated under tension and compression stress states. The highest transformation strains are found under pseudoelasticity for the [0 0 1] orientation in tension and compression as 6.2% and 4.1% respectively. Experiments reveal tension–compression asymmetry of the critical transformation stress and of the stress hysteresis. The pseudoelastic stress–strain response is limited in tension to a much narrower temperature range than that in compression. The levels of strain recovery and the size of the stress hysteresis reveal the influence of dissipative mechanisms. A thermodynamics framework is proposed for describing the role of plastic flow and the internal stress fields on the stress hysteresis behavior. Single crystals exhibit considerable recovery compared to polycrystals and multicrystals. Extensive transmission electron microscopy results confirm the increased plastic flow at the austenite–martensite interfaces and in the secondary phase.


*Keywords:* Shape memory; Pseudoelasticity; Critical stress; Phase transformation; Ferromagnetic shape memory alloy

## 1. Introduction

Ferromagnetic shape memory alloys (FSMAs) such as CoNiAl have potential for rapid actuation and sensing which expands the current use of shape memory alloys (SMAs) to applications requiring a higher frequency response [1]. It is well known that the applied magnetic energy needs to overcome the elastic stored energy in order for magnetic field-induced shape changes to occur. Therefore, it is important to understand the deformation response of CoNiAl under different stress states, such as tension and compression. Previously, only compressive response was considered due to the perceived lack of ductility in these materials [1–6]. Recently, Sehitoglu and coworkers [7] revealed large pseudoelastic strains near 8% under tension in single crystals. In the present paper, we present the results of a large experimental program (nearly 100 experiments) on single-crystal CoNiAl under tension and compression and compare them to the polycrystalline response in compression. Unlike single crystals, the aged polycrystals exhibit brittle behavior under tension and do not exhibit pseudoelasticity. In an effort to obtain tensile results for comparison, multicrystals (including bicrystals) are investigated under tension and compression. We expose the tension–compression asymmetries in critical stress, transformation strains, and stress hysteresis.

We focus on CoNi33Al27 (at.%) aged at 1275 °C for 3 h. Tension–compression results are presented for the orientations [0 0 1] and [1 1 5] of single crystals and multicrystals of nominally [1 2 3] orientation ([1 2 3]N). For comparison, randomly oriented polycrystalline results in compression are also included. In addition to achieving pseudoelasticity in tension, nominally [1 2 3] oriented multicrystals are studied to ascertain the influence of texture. The multicrystals are distinguished from polycrystals, in that they consist of primarily 2–4 crystal orientations with the predominant orientation being [1 2 3]. The multicrystals provide insight

* Corresponding author.
*E-mail address:* huseyin@uiuc.edu (H. Sehitoglu).

1359-6454/$30.00 
doi:10.1016/j.actamat.2005.09.025

into the effects of texture in that the intergranular constraint is severely relaxed compared to the completely random polycrystalline alloys. In fact, we observe distinct pseudoelastic response in the [1 2 3]N multicrystals in tension and compression, whereas it is completely absent in the polycrystals for both stress states.

The secondary phase promotes higher ductility in these alloys [1,8]; however, it does not participate in the transformation. Microscopy images reveal that the second phase undergoes severe plastic deformation. It is possible to achieve a single-phase microstructure with higher temperature annealing treatments but these treatments produce higher strength which increases the propensity of brittle response in tension. Higher strength yields higher critical transformation stresses, which are unsuitable for magnetic shape memory applications. Through this study, we provide a better understanding of the orientation effects and of the non-transforming second phase.

The purpose of this work is to characterize the tension–compression asymmetry of single-crystal two-phase ($\gamma$ and $\beta$) CoNi33Al27 at temperatures above the austenite finish temperature ($A_f$) and explain the origins of the difference. We present the theoretical correspondent variant pair (CVP) tension and compression transformation strains to compare to the experimentally determined values in the presence of the second phase. The orientation dependence of the CVP strains was determined using the energy minimization method explained in detail in our previous work [7]. The lattice constants for this particular composition [7] were used in the calculations; however, the results are similar if the lattice constants reported in the literature are utilized [3]. We present the compression results for the first time. Most noticeably, we find that, although the theoretical CVP strains are not achieved in tension, they are slightly exceeded in compression despite the second phase constituent. Tension–compression asymmetry and orientation dependence was studied using three experimental methods: (1) repeated cycling at 2% strain, (2) incremental increase in applied strain from 2% to 8% strain, and (3) temperature cycling under stress. Cyclic strain experiments were conducted at 50, 75, and 100 °C to stress-induce transformations under pseudoelasticity conditions and establish the pseudoelastic window. In addition to using the transformation to describe the tension–compression asymmetry, we report on the critical stress, pseudoelastic recovery, and stress hysteresis.

There are a number of unusual findings associated with the heat-treated (3 h at 1275 °C) CoNi33Al27 (at.%) alloys that do not conform to our usual understanding of the traditional SMAs. We briefly describe these differences now. First, the presence of a non-transforming secondary phase is reminiscent of precipitates in NiTi alloys. However, unlike the precipitates, the secondary phase undergoes considerable plastic deformation as evidenced by transmission electron microscopy (TEM; to be reported later in the paper). Second, the presence of the plastically deformed second phase is beneficial in extending the ductility of this class of alloys. Contrary to previous polycrystalline materials [1], the presence of plastic deformation does not cause a drastic critical stress decrease due to cyclic loading for the single-crystal materials, which display remarkable stability in tension and compression. Third, there is a large asymmetry in the slope of the Clausius–Clapeyron curve in tension and compression, which cannot be solely attributed to the difference in transformation strain magnitudes [9,10]. This points to the presence of high internal stresses in the matrix that modify the critical stress–temperature relationship. Another, more outstanding feature is that the CoNiAl undergoes a finite volume change of near 4% while traditional shape memory materials exhibit very small volume change during the transformation [7]. Despite this large volume change the material exhibits remarkable pseudoelastic strain reaching values as high as 6.2%. Exceptional recoverable strains are observed in both tension and compression despite the large volume change, and also recoverability increases with cyclic loading. Utilizing a thermodynamic formulation [10–15], we derive an expression for the stress hysteresis. Based on this model we explain the contributions to the stress hysteresis. To gain further understanding, we compare the stress hysteresis from the isothermal stress–strain experiments to the thermal hysteresis from isostress (constant stress) thermal cycling experiments. We provide insight into dissipative mechanisms through evaluation of recoverable strain and of the stress hysteresis considering the non-transforming second phase and the large volume change.

## 2. Modeling of stress hysteresis

A complementary free energy equation for a multivariant martensitic transformation is given by [11–15]

$$\Psi(\Sigma_{ij},T,f_n) = -B(T-T_0)\sum_n f_n + \tfrac{1}{2}\Sigma_{ij}E^{\mathrm{e}}_{ij} + \Sigma_{ij}\sum_n \varepsilon^n_{ij} f_n - \sum_{n,m} H^{nm} f_n f_m, \tag{1}$$

where $H^{nm}$ represents the energy contribution due to interaction between two variants $m$ and $n$. The total resistive term $\sum_{n,m} H^{nm} f_n f_m$ arises from martensite variant interactions between existing martensite variants and a nucleating one. The term $B(T-T_0)$ is the chemical energy difference between austenite and martensite where $T_0$ is the equilibrium temperature. The term $\Sigma_{ij}E^{\mathrm{e}}_{ij}$ represents the energy contribution from the macroscopic external stresses, and the term $\Sigma_{ij}\sum_n \varepsilon^n_{ij} f_n$ represents the interaction energy between the external stress and the transformation strains. The transformation conditions for the forward and reverse transformations are obtained by taking derivatives with respect to volume fraction $f_n$:

$$\begin{aligned} F^{\mathrm{C}} &= \Sigma^{\mathrm{F}}_{ij}\varepsilon^n_{ij} - \sum_m H^{nm} f_m - B(T-T_0), \\ -F^{\mathrm{C}} &= \Sigma^{\mathrm{R}}_{ij}\alpha\varepsilon^n_{ij} - \sum_m \alpha^2 H^{nm} f_m - B(T-T_0), \end{aligned} \tag{2}$$

where $F^C$ is the critical value of the transformation driving force. The term $\alpha$ modifies the transformation strain in the reverse transformation case because of dissipative mechanisms. $\Sigma_{ij}^F$ and $\Sigma_{ij}^R$ represent the forward and reverse transformation stress levels respectively. Subtracting the second equation from the first, the stress hysteresis can be expressed as

$$\left(\Sigma_{ij}^F - \Sigma_{ij}^R\right)\varepsilon_{ij}^n = F^C\left(1+\frac{1}{\alpha}\right) + \sum_m H^{nm} f_m(1-\alpha) + B(T-T_0)\left(1-\frac{1}{\alpha}\right). \quad (3)$$

In Eq. (3), the chemical free energy term can be modified using the well-known Clausius–Clapeyron equation as $B = \varepsilon_0(\mathrm{d}\Sigma_{cr}/\mathrm{d}T)$ where $\varepsilon_0$ is the maximum transformation strain resolved in the direction of loading.

The final equation for the stress hysteresis for the uniaxial case can be expressed as

$$\left(\Sigma^F - \Sigma^R\right)\varepsilon_0 = F^C\left(1+\frac{1}{\alpha}\right) + \sum_m H^{nm} f_m(1-\alpha) - \varepsilon_0 \times \frac{\mathrm{d}\Sigma_{cr}}{\mathrm{d}T}(T-T_0)\left(\frac{1}{\alpha}-1\right). \quad (4)$$

The three terms on the right-hand side help clarify the influence of frictional resistance, variant interaction, and matrix strength on the stress hysteresis. The frictional resistance (first term) to the transformation is an irreversible mechanism so it is an additive contribution that promotes higher stress hysteresis. Likewise, variant–variant interaction is a dissipative mechanism that increases the hysteresis so the second term is additive. The slope of the temperature dependence of the critical stress relation, $\mathrm{d}\Sigma_{cr}/\mathrm{d}T$, reflects the strength of the parent phase with respect to temperature. If $\varepsilon_0(\mathrm{d}\Sigma_{cr}/\mathrm{d}T)$ is high the stress hysteresis is decreased due to the third term as follows. Strengthening mechanisms that promote high $\mathrm{d}\Sigma_{cr}/\mathrm{d}T$ levels are accompanied by high elastic energy storage. Elastic energy stored during the forward transformation assists the reverse transformation and hence it helps decrease the stress hysteresis. In addition, matrix strengthening suppresses dislocation nucleation. Therefore, the third term is a negative contribution to the hysteresis.

The term $\alpha$ is a qualitative measure of the effect of plastic relaxation. As discussed by Hamilton et al. [15], upon plastic relaxation, the modified transformation strain is $\varepsilon_{ij}^{n*} = \alpha\varepsilon_{ij}^n$. When $\alpha$ is 0, the transformation strain is accommodated plastically and the reverse transformation is prohibited. When $\alpha$ is 1, the transformation strain is completely accommodated elastically. With respect to Eq. (4), when $\alpha$ is 0, the first and third terms cancel and the stress hysteresis is attributed to the interaction of plastically accommodated martensite variants. The terms in the $H^{nm}$ matrix for this case have the values for incompatible variants, $\mu/150$. For a typical shear modulus of 50 GPa, after summation over 24 variants, the stress hysteresis is of the order of 1 GPa. Such a value for the stress hysteresis far exceeds the yield strength of austenite, so this means a stress hysteresis is not observed and the reverse transformation does not occur. Note that in the absence of dislocation emission at the austenite–martensite interfaces (i.e., $\alpha = 1$), Eq. (4) reduces to the form given by Siredey et al. [14] as $F^C = \frac{1}{2}\left(\Sigma^F - \Sigma^R\right)\varepsilon_0$.

## 3. Experimental methods and materials

Single-crystal CoNi33Al27 (at.%) samples were grown using the Bridgman technique in an inert environment. The [0 0 1], [1 2 3], and [1 1 5] orientations were selected for experiments because of the varying degree of CVP formation (in the range 2–8) and the number of active slip systems present for each orientation. Martensite is known to be composed of internal twins, i.e., twin-related CVPs form. The [0 0 1] orientation cannot undergo slip because of the lack of slip systems. Thus it is expected to demonstrate the smallest stress hysteresis of all orientations. However, CVP interaction will be most significant for the [0 0 1] orientation, as the highest number of active variants form in this orientation. The [1 1 5] orientation is similar to the [0 0 1] case, in that it has multiple active CVPs and high resolved shear stress factors (RSSFs) compared to the [1 2 3] orientation, without the limits on the slip systems. The [1 2 3] orientation exhibits a single variant, which will minimize CVP interaction to highlight the intergranular effects in the multicrystals. The [1 2 3]N orientation represents nominally [1 2 3] crystals including bicrystals near the [1 2 3] direction.

The transformation temperatures of the two-phase alloy were determined using differential scanning calorimetry (DSC). Samples for DSC weighed approximately 100 mg and were thermally cycled in the calorimeter at 40 °C/min. DSC results were obtained for annealing temperatures of 1200, 1275, and 1350 °C with annealing times varying from 0.5 to 48 h. A total of 40 cases were considered and a brief summary of the results is given in Fig. 1. The peaks of the calorimetry curves for the sample heat treated at 1275 °C for 3 h were at 6 °C for the forward transformation and 31 °C for the reverse transformation. Therefore, the thermal hysteresis (measured from peak to peak) is approximately 25 °C. This value of thermal hysteresis is comparable to that of the well-known NiTi alloys. Based on these results, the 1275 °C/3 h heat treatment was chosen as the heat treatment for mechanical experiments because the transformation occurred nearest to room temperature and exhibited a narrow hysteresis.

The eutectic-like microstructure consisting of $\gamma + \beta$ phases is shown in the scanning electron microscopy image in Fig. 2. The austenite, $\beta$, has a B2 crystal structure that transforms to martensite, $\beta'$, which has an $L1_0$ crystal structure. To identify the phase constitutions, specimens were prepared for optical microscopy by electropolishing using hydrochloric acid and methanol in equal parts as an electrolyte. Other electropolishing operating parameters include: approximately 10–20 V, 4 A/mm$^2$, 25 °C. After

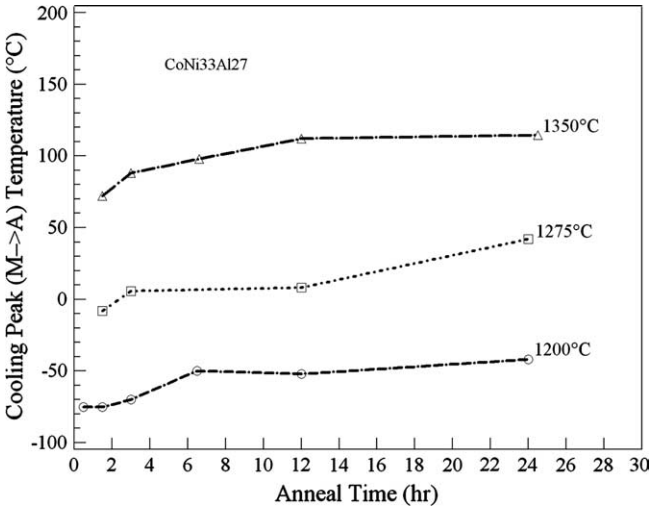


Fig. 1. Peak temperatures determined using differential scanning calorimetry (DSC) showing the forward transformation temperature variations as a function of annealing temperature and time.

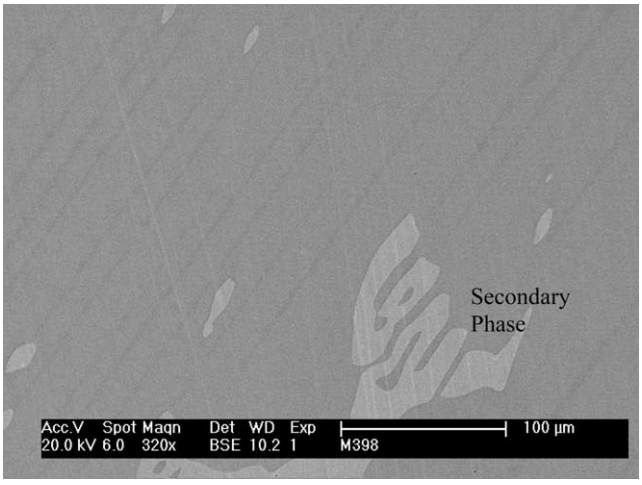


Fig. 2. Scanning electron microscope (SEM) image of the secondary phase in CoNiAl and the parallel dark thin bands are residual martensite plates. The martensite plates impinge on the second phase and in regions where the second phase is absent, the martensite growth proceeds uninhibited.

thermal cycling under constant uniaxial tensile loading, an energy dispersion X-ray spectroscopy (EDX) analysis was performed to resolve the chemistry of the phases present. Table 1 contains the results showing that the Al content in the secondary phase, $\gamma$, is 13.3% while the Al composition in the B2 matrix was measured as 23.6%. The A1 disordered $\gamma$ phase is known to enhance ductility [1–7] and produces a modified internal stress field [1,3]. Relative to the matrix and plate phases, the second phase contained half the amount of Al, 13 at.% more Co, and an equivalent concentration of Ni. The depletion of Co from the matrix increases the transformation temperatures for higher aging temperatures [3,15], and this is exactly reflected in the DSC peaks (Fig. 1). For higher temperatures and longer aging times, the transformation temperatures increase.

Table 1
Shows measurement of chemical composition in the austenite matrix, secondary, and martensitic phases

| Phase | Chemistry (at.%) | | |
|---|---|---|---|
| | Al | Co | Ni |
| Matrix | 23.6 | 40.1 | 36.3 |
| Secondary | 13.3 | 53.6 | 33.1 |
| Martensite | 22.9 | 40.5 | 36.6 |

In addition to the $\gamma + \beta$ phases shown in Fig. 2, residual martensite also appears in the TEM images shown in Fig. 3(a) and (c). This indicates some irreversibility is generated by the transformation and its interaction with the $\gamma$ phase. Thus martensite is stabilized after the phase transformation is complete. Fig. 3(a) shows a TEM image of an interface between martensite and the $\gamma$ phase. The internal twins are thin, and, interestingly, the $\gamma$ phase has a high dislocation density. As indicated by the arrows, those dislocations may be inherited by the transforming martensite. When this is the case, the dislocations relax the stored elastic strain energy and create additional frictional resistance to the reverse transformation. Because it does not undergo transformation, the $\gamma$ phase can interfere with twin boundary motion and our prior studies shows that martensite can be trapped as a result [1,7], and less material undergoes the transformation. For those reasons, the $\gamma$ phase also inhibits theoretical transformation strain levels from being attained. A final noteworthy observation is that Fig. 3(b) and (c) show a stark contrast in dislocation density in the parent phase, which is far less than the second phase in the single crystals. The diminished dislocation activity in the parent phase is linked to the good recoverability.

Compression and tension mechanical experiments were conducted using a servohydraulic load frame and strain was measured with a miniature extensometer with a 3 mm gauge length. Small-scale compression specimens (4 mm × 4 mm × 10 mm) were electrodischarge machined from the cast ingot. Dog-bone-type, small-scale tension specimens were electrodischarge machined from the ingot to have an 8 mm (height) × 3 mm (width) × 1.5 mm (thickness) gauge section. Stress–strain tests were conducted under strain control at $10^{-4}$/s. However, in cases where abrupt stress drops occurred during the transformation, position (displacement) control was utilized instead to avoid overloading of the samples. After unloading, when residual strains remain, they were recovered by heating to approximately 70 °C above $A_f$ and then cooling back to the test temperature. Even after the heat–cool cycle, a small unrecoverable strain remains indicating some irreversibility, which was monitored for each stress–strain cycle. Isostress thermal cycling started with the load applied above $A_f$, to ensure the specimen was fully austenitic, followed by cooling until the transformation strain saturated, and finally the specimen was heated until the recovery strain saturated. Heating and cooling rates were approximately 10 °C/min to promote uniform temperature changes throughout the specimen. The external stress was increased

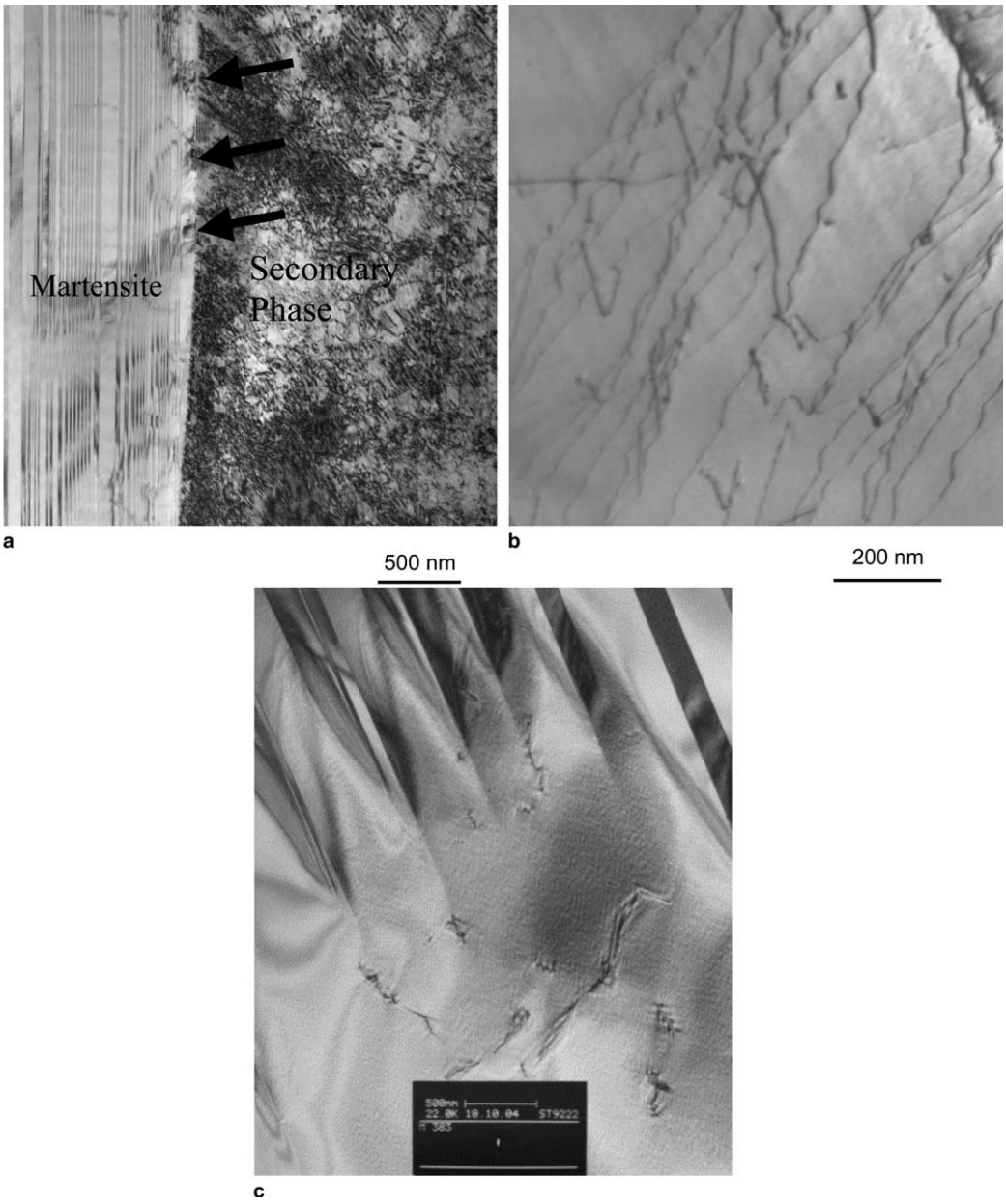


Fig. 3. (a) Transmission electron microscopy (TEM) bright field image of martensite next to a second phase boundary showing a high density dislocations in the second phase and arrows indicate that dislocations may be inherited by impinged martensite, (b) TEM bright field image of dislocations in the matrix phase and (c) Isolated dislocations in CoNiAl and the lamellar structure in the background is residual martensite.

incrementally until either the transformation strain saturated or the specimen showed a significant level of unrecoverable (plastic) strain.

## 4. Results

The influences of the stress direction and crystal orientation on the temperature dependence of the critical stress are distinguished utilizing Fig. 4. In clear agreement with the well-known Clausius–Clapeyron relation, we find that for each orientation the critical stress increases with temperature, and in compression, the increase is much greater than in tension. This is illustrated by the different slopes under compression (4.1 MPa/°C) and tension (1.3 MPa/°C). The different slopes deserve close scrutiny because they relate to the driving force required to initiate the forward transformation at a given temperature, as well as the stress hysteresis. Similar to the present findings, previous work established the slope of the Clausius–Clayperon curve as 4.2 MPa/°C under compression for a polycrystal CoNiAl alloy [1]. Fig. 4 also displays the orientation dependence of the critical stress magnitude: the critical stress is similar for the [0 0 1] and [1 1 5] orientations, while the nominally [1 2 3] orientation multicrystals exhibit a higher critical

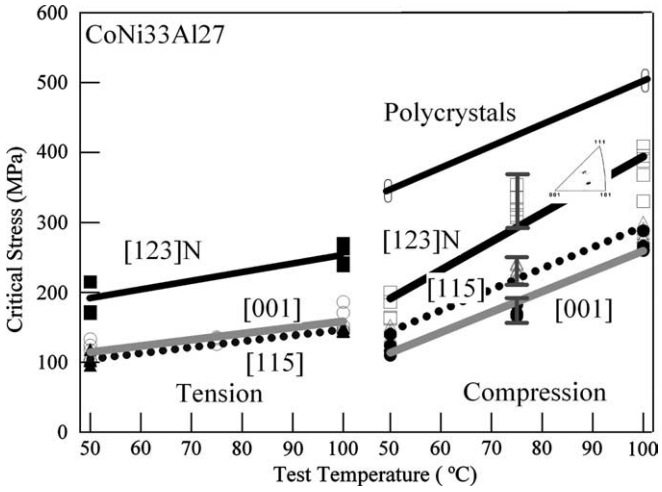


Fig. 4. The critical transformation stress for the [0 0 1] and [1 1 5] orientations and nominally [1 2 3] multicrystals. Results are from isothermal cyclic stress–strain experiments up to 2% strain with the first five cycles shown in the plot. The critical transformation stress is higher under compression compared to tension with a more noticeable difference at 100 °C. The critical stress is similar for the [0 0 1] and [1 1 5] orientations while the orientations labeled N[1 2 3] exhibit higher critical stress at each test temperature under tension and compression. The polycrystalline material shows the highest critical stresses in compression. The change in critical stress with cycling is the lowest for the single crystals.

stress under tension and compression at each test temperature. The polycrystalline case achieves the highest critical stresses under compression. Clearly the intergranular constraint causes elevated critical stress levels, because as it is relaxed for the multicrystals, the critical stress decreases. It is interesting to note that discrepancies between tension and compression critical stress magnitudes at 100 °C far exceed those at the 50 and 75 °C. We provide a plausible explanation for this later in the discussion.

In addition to comparing the magnitude of the critical forward transformation stress under tension and compression at the different test temperatures, we also compare its evolution with cycling. Fig. 5 shows the decrease in critical stress for the [1 1 5] orientation at 50 and 100 °C loaded under compression. At 50 °C under compression, the critical stress decreases approximately 18%. At higher test temperatures, the change in critical stress is smaller and near 5%. The critical stress experiences a similar small decrease at 50 °C in tension for the [1 1 5] single crystal (Fig. 6). In a prior study on CoNiAl polycrystals, we found that cycling decreased the critical stress as increased dislocations remained in the re-transformed austenite matrix [1]. The decrease in critical stress (~18%), near $A_f$ at 50 °C, is far below that found for polycrystals (~70%) [1]. From Fig. 4, we make further observations regarding the change in critical stress with cycling. The bars for the 75 °C temperature in compression illustrate the general trend for each test temperature: The nominally [1 2 3] multicrystals exhibit the largest change, whereas the change is smaller and equivalent for the [0 0 1] and [1 1 5] single crystals. The relatively stable cyclic stress–strain response at 50, 75, and 100 °C for the [0 0 1] and [1 1 5] orientations in tension and compression is quite remarkable and illustrates the importance of texture.

Further insight into asymmetry is illustrated by the transformation strain recovery under tension and compression in Figs. 6 and 7. Since all test temperatures are above the reverse transformation temperature, a pseudoelastic

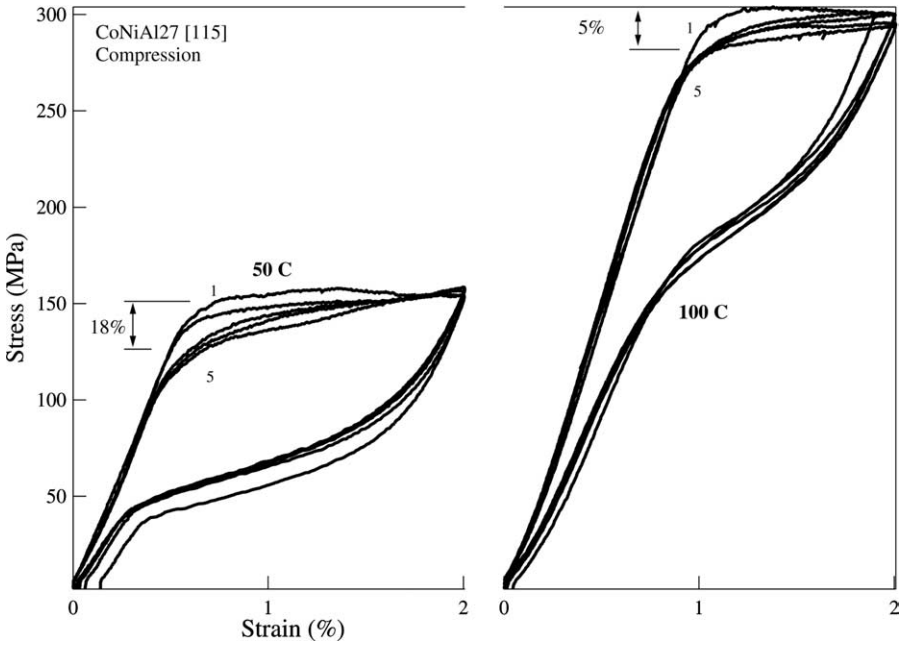


Fig. 5. Cyclic stress–strain curves of the [1 1 5] orientation under compression at 50 and 100 °C showing approximately 18% and 5% decrease in critical stress respectively.

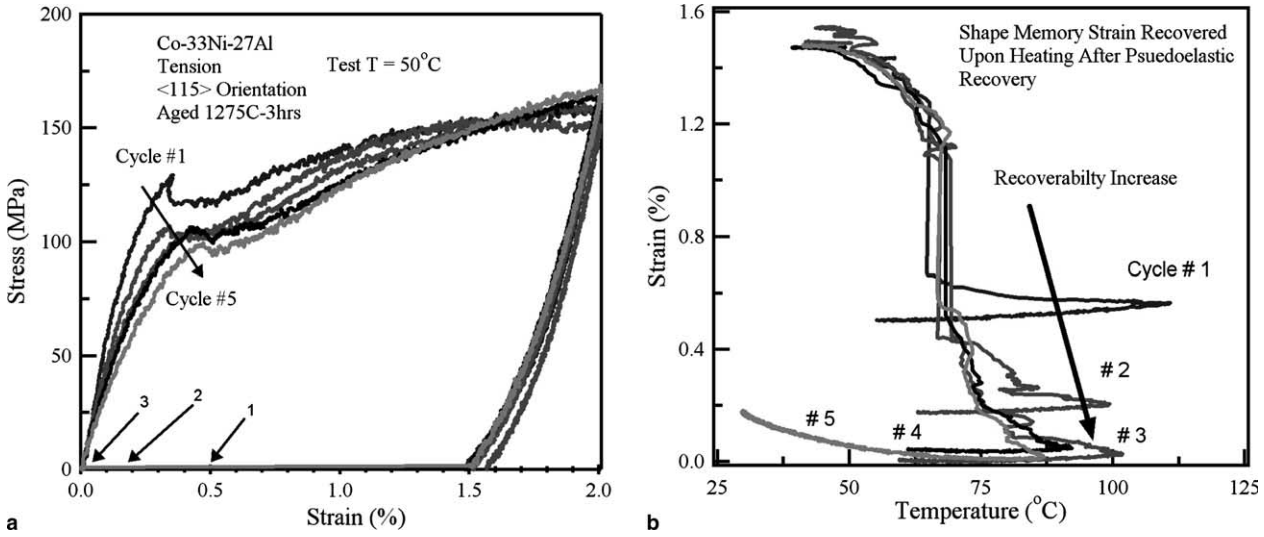


Fig. 6. (a) Stress–strain response at a test temperature of 50 °C showing an increase in recoverability near $M_s$ from cycle #1 to #5 and (b) increasing shape memory strain recovery upon heating.

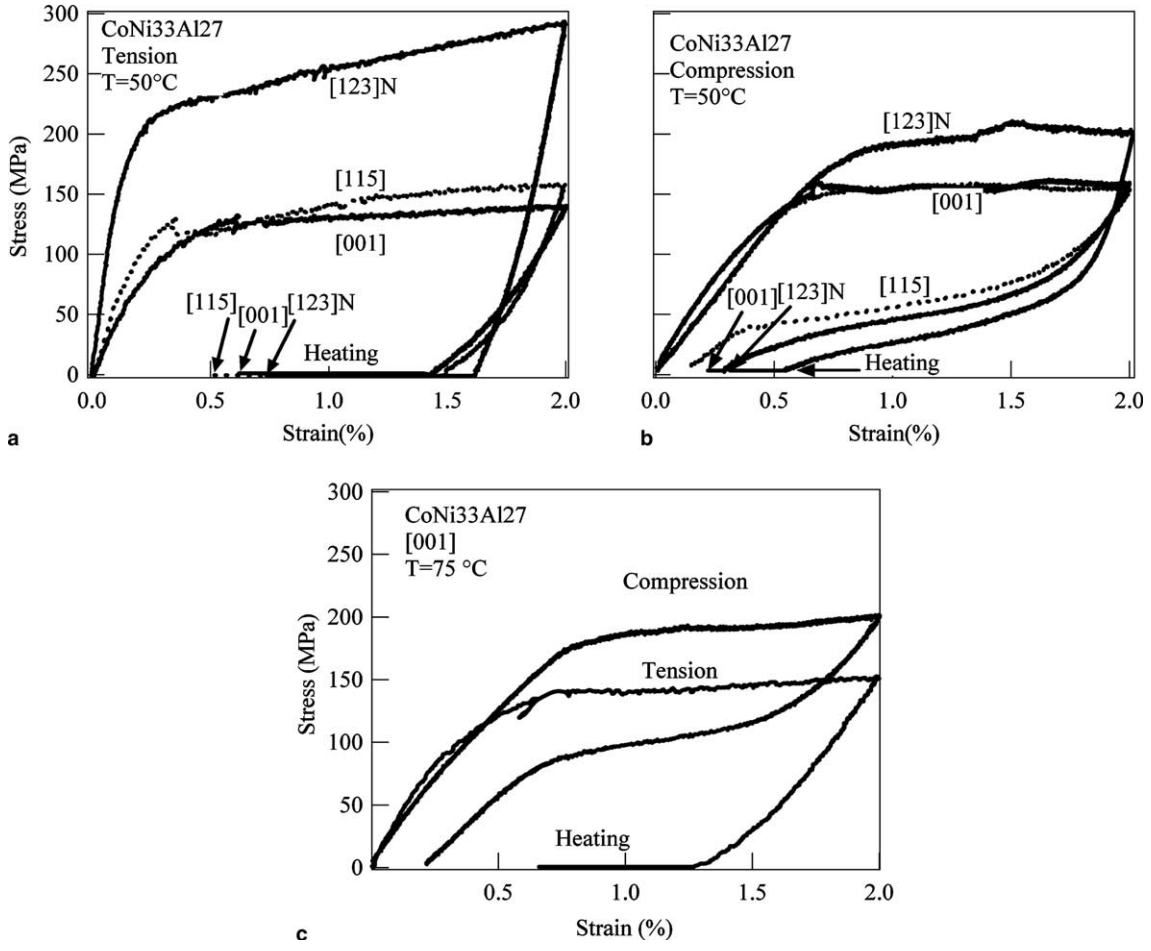


Fig. 7. (a) Tension and (b) compression stress–strain curves at 50 °C showing almost perfect pseudoelasticity under compression and very little under tension. The critical stress is comparable for the [0 0 1] and [1 1 5] orientations with it being slightly higher in compression. The nominally [1 2 3]N oriented multicrystals exhibit higher critical stress under tension and compression. (c) Results for [0 0 1] orientation at 75 °C also showing the pseudoleasticity in compression relative to tension. Note that the compressive critical stress becomes noticeably higher than that of tension at 75 °C.

stress–strain response is expected. Fig. 7 shows the stress–strain results for the first cycle. Interestingly, at 50 and 75 °C, under tension there is small pseudoelastic recovery and the remaining strain recovers upon heating at zero load due to the shape memory effect (SME). Under compression, nearly all of the deformation is recovered

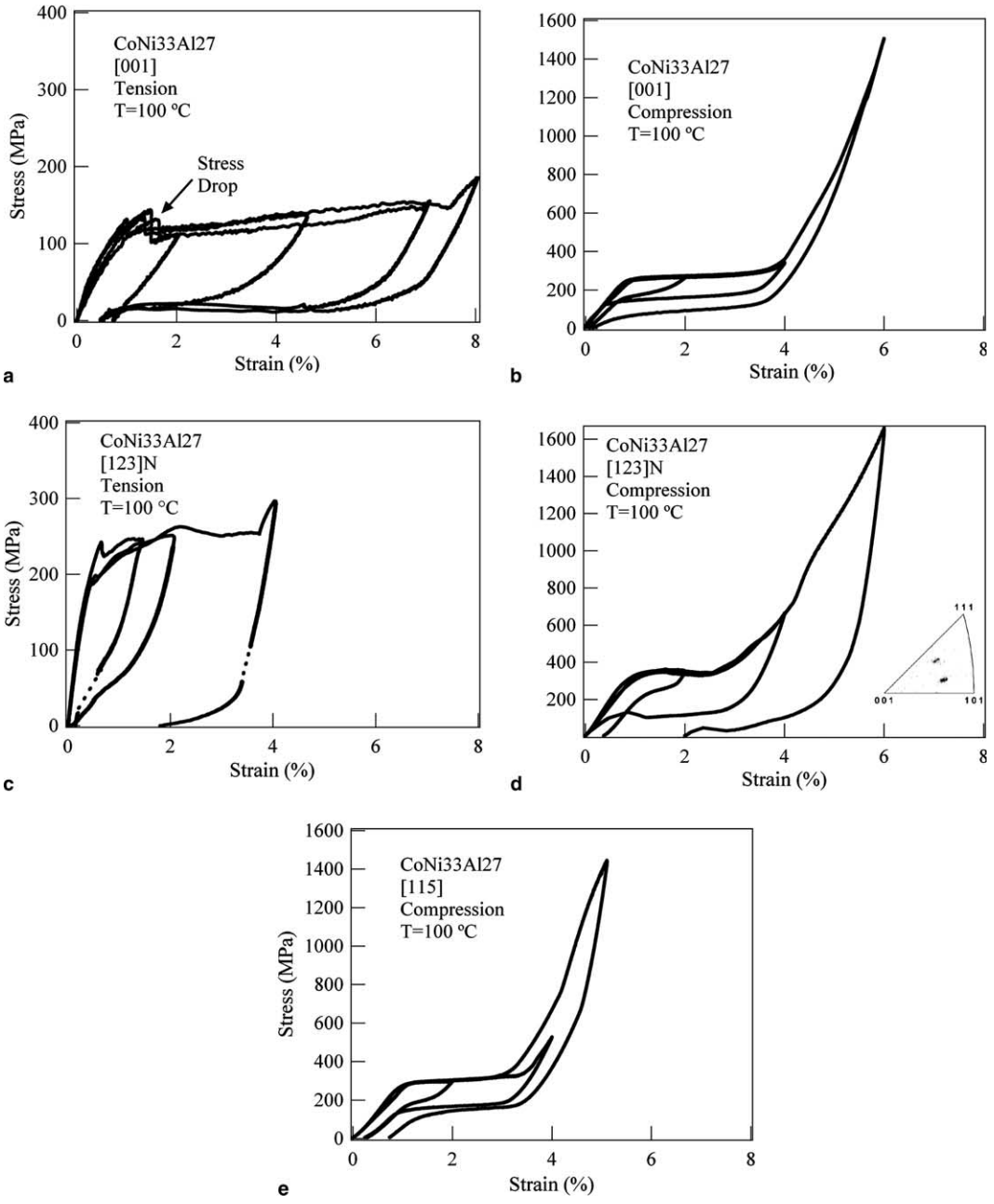


Fig. 8. Stress–strain curves of incrementally increasing deformation above $A_f$ (100 °C) for: [0 0 1] single crystals in tension (a) and compression (b); nominally [1 2 3] multicrystals in tension (c) and compression (d); and [1 1 5] single crystals in compression (e). Results show that maximum transformation strains are higher under tension compared to compression, and the critical stress is higher for compression. The largest tensile transformation strains (6.2%) are found for the [0 0 1] orientation (a) and the smallest tensile transformation strains (3.8 %) are found for the [1 2 3]N orientation (c). Similarly, the [0 0 1] orientation (c) exhibits the largest compressive strains (4.1 %) and the [1 2 3]N orientation (d) exhibits the smallest. In tension, there is a stress drop prior to the plateau stress that is not present in compression for the single crystal alloys.

pseudoelastically. Meanwhile at 100 °C under tension and compression (Fig. 8), the recovery is predominately pseudoelastic for the single crystals. Comparing Fig. 7(a) and (b), we note that even after heating to recover strains via the SME, compressive transformation strains exhibit more recovery. This result is of particular interest for the [0 0 1] and [1 1 5] cases in view of the similar stress levels in tension versus compression. The results indicate that at 50 and 75 °C under tension the martensite is stabilized and hence it remains after unloading and a thermal driving force is required to complete the reversion to austenite via the SME. In compression, the martensite is not stabilized during unloading so the reverse transformation occurs via pseudoelasticity. To gain further insight into the results, we studied the residual transformation strains with cycling. Fig. 6(b) illustrates increasing SME recovery near $A_f$ in tension for the [1 1 5] orientation, considering the difference between cycles 1 and 5. As the recovery increases, the transformation stress is relatively stable for strains near 2% from cycles 2 to 5. Fig. 5 shows that for the same orientation and

test temperature, in compression, the pseudoelastic recovery also increases with cycling. Similar to the tensile case, the transformation stress exhibits remarkable stability. Clearly the single-crystal alloys exhibit resilience against degradation that is remarkable relative to the polycrystal alloys.

For the incremental strain cycling, performed at 100 °C, we further characterize the tension–compression asymmetry considering the transformation strains. The maximum transformation strains are determined from the stress–strain curves by subtracting the elastic recovery portion. This elastic recovery is estimated by extrapolating the linear unloading portion of the stress–strain curve to zero stress. Theoretical compressive transformation strain contours indicating the orientation dependence are given in Fig. 9. Experimental transformation strains follow the theoretical predictions closely as shown in Table 2. The theoretical results shown in Table 2 are arrived at based on the energy minimization theory of martensitic transformation [7]. The transformation strains are higher under tension compared to compression for every orientation. The [0 0 1] orientation displayed the largest transformation strain under tension (6.2%) and under compression (4.1%). In contrast, the [1 2 3]N oriented multicrystals displayed the smallest transformation strain under tension (3.8%) and under compression (3.3%). The results show that in tension CVP strains are not achievable in the presence of the second phase, while in compression they are exceeded. Consequently, it is more likely that detwinning occurs in compression because CVP strains are exceeded and detwinning is much less prevalent in tension. We rationalize the stress hysteresis later considering this difference.

We quantitatively examine the stress hysteresis in terms of the magnitude for each strain increment and report the orientation and stress-state dependence. The stress hysteresis increases with increased applied strain for all orientations under compression and tension (shown in Fig. 10). Fig. 10 shows the stress hysteresis under tension and compression for the [0 0 1] and [1 1 5] single crystals and [1 2 3]N multicrystals at 2%, 4%, and 6% applied strain. The stress hysteresis is always lower in tension compared to compression (Fig. 10). Note that a small tension–compression asymmetry of the stress hysteresis exists at 2% strain. The tension–compression asymmetry increases dramatically with increasing applied strain and the hysteresis grows markedly from 2% to 6% strain under compression. Under compression the stress hysteresis grows more rapidly with applied strain compared to tension loading (i.e., greater slope). Although all orientations display the aforementioned behavior, it is far more pronounced for the nominally [1 2 3] orientated crystals. From Fig. 10, the hysteresis growth for the [1 2 3]N orientation is 112 MPa under tension and 247 MPa under compression, while for the

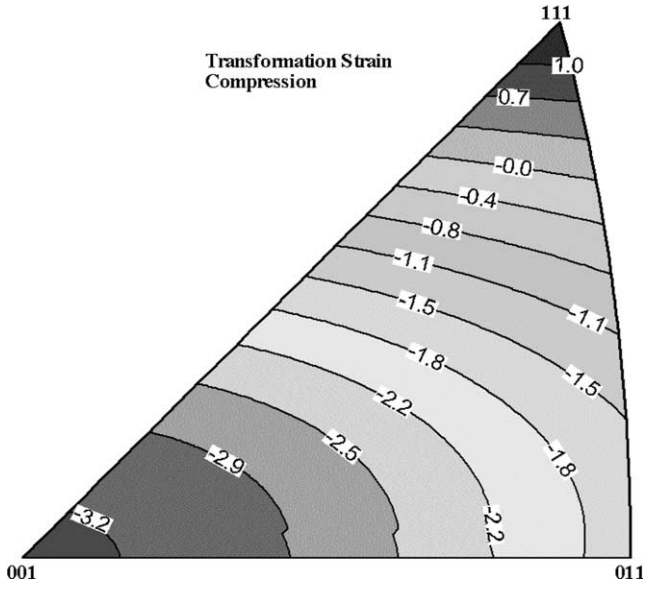


Fig. 9. Theoretical contours of transformation strain in compression. The contours for tension can be found in [7].

Table 2
Experimentally determined maximum transformation strains and theoretical transformation strains without detwinning for the orientations studied in the current work

| Orientation | CVP transformation strains (%) | | | |
|---|---|---|---|---|
| | Tension | | Compression | |
| | Theoretical | Experimental | Theoretical | Experimental |
| [0 0 1] | 8.4 | 6.2 | 3.3 | 4.1 |
| [1 1 5] | 7.8 | 5.5 | 2.7 | 3.3 |
| [1 2 3] | 5.5 | 3.8 | 1.6 | 3.3 |

Note that for the [1 2 3] case, the experimental values are for the [1 2 3]N multi-crystals.

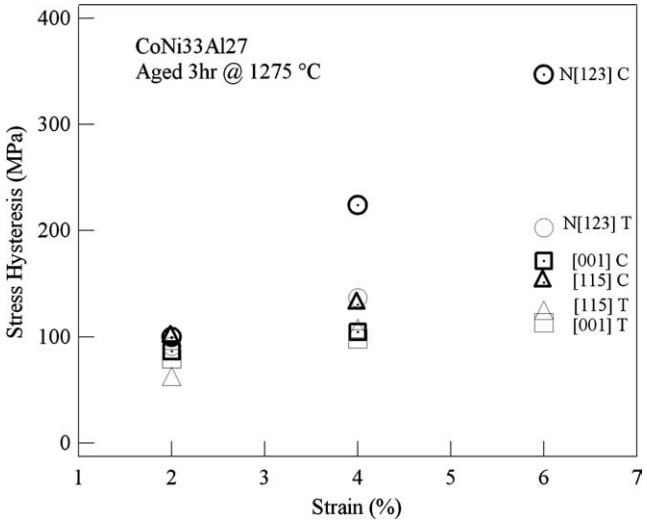


Fig. 10. Stress hysteresis in tension (T) and compression (C), bold shapes with centered dots, as obtained in experiments with incremental increase in strain. The stress hysteresis is determined from stress–strain curves shown in Fig. 8 at approximately half of the applied strain.

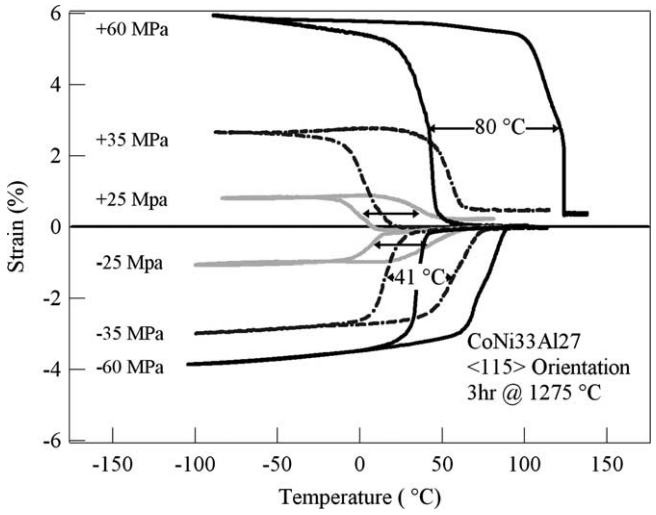


Fig. 11. The thermal hysteresis growth, measured at half the transformation strain as indicated by arrows, with increasing tensile and compressive isostress for an aged CoNiAl single crystal. The temperature hysteresis and transformation strain are equivalent for the 25 MPa stress for the two stress states, but the width of the hysteresis evolves remarkably different for the two stress modes. For the tension case, the hysteresis grows approximately 50 °C, which is considerably larger than its growth in compression (~9 °C).

[0 0 1] orientation it is 33 MPa under tension and 88 MPa under compression. These results point to large variations in stress hysteresis as a function of external stress direction and crystal orientation.

The thermal hysteresis shows the opposite trend (Fig. 11). The compressive temperature hysteresis is smaller than that of the tensile case. The stresses for the strain–temperature results are much lower than those achieved in the stress–strain experiments. In our previous work, we remarked that contrasting variant interactions occur during martensite growth for isothermal stress–strain versus isostress thermal cycling at such low stresses [7]. A higher occurrence of internal and external stress-induced variant interactions and more significant second-phase impingement are expected for the low stresses. However, at isothermal test temperatures above $A_f$ single variants are induced exclusively because higher stresses curtail the influence of second-phase internal stress fields. We elaborate on contrasting energetic contributions that arise because of variant interaction in the discussion.

In addition to the stress hysteresis, the evolution of the residual strain with increasing incremental deformation offers another means to assess irreversibility. The stress–strain behavior of the [0 0 1] orientation shown in Fig. 8(a) and (b) strikingly indicates dissipation with a constant residual strain. This is understood by the increase in stress hysteresis from 4% to 6% strain and almost complete recovery upon unloading in compression (Fig. 8(b)) and constant residual strain in tension (Fig. 8(a)). The [1 1 5] orientation exhibits higher residual strain and it increases in compression (Fig. 8(e)). The stress–strain behavior of the [1 2 3]N multicrystal shows an increase in residual strain (shown in Fig. 8 (c) and (d) for tension and compression). Since the [1 2 3]N was loaded under compression to 4%, well beyond the theoretical 2.1%, a large unrecoverable strain of 2% remains. In compression high stress levels (above the plateau stress) can be applied unlike in tension where fracture occurs. The noticeable stress drop, illustrated in Fig. 8(a), occurs at the onset of the forward transformation in tension and does not appear under compression. While the residual strain remains after completion of the transformation, this observation shows that the deformation mechanisms differ in tension and compression from the onset of the transformation.

## 5. Discussion

The critical stress increases for elevated temperatures, which is typical of SMAs reported in the literature. However, we observe a substantially higher increase in critical stress with increasing temperature in compression than in tension. The relatively high increase in critical stress in compression relative to tension is partially attributed to the smaller value of the transformation strain in compression [16]. However, the results demonstrate a threefold increase in stress (or slope in Fig. 4) which is unusual. The asymmetry is likely enhanced due to the additional contribution the second phase provides to the resolved shear stress on a CVP. A similar effect attributed to precipitates has been reported in a previous study on NiTi [9]. Hamilton et al. note that the volumetric strain increases the mechanical energy contribution in tension [7]. As a result, the critical stress levels are lower for tension and thus a smaller increase in magnitude with higher temperature is expected. The polycrystalline material exhibits remarkably higher transformation stresses in compression and the single crystals exhibit the lowest, while the multicrystal stresses provide the intermediate values. The polycrystal results clearly illustrate that the intergranular constraint stabilizes the austenite, and this effect can be relieved through texturing as reflected in the nominally [1 2 3] multicrystal response.

The critical stress decreases during cycling for all orientations (Figs. 5 and 6). Multicrystals of nominally [1 2 3] orientation experience a greater decrease than the [0 0 1] and [1 1 5] single crystals. This can partly be due to the additional defects created by grain constraint and grain boundaries. The cause of this decrease is often linked to the stress fields of the residual martensite trapped by these dislocations which acts to orient preferentially the nucleating variants of martensite to the externally applied stress, thus facilitating the subsequent transformation cycles [1]. During pseudoelastic cycling, the internal stress fields assist the driving force for the forward transformation in subsequent cycles and thus the critical stress decreases. At 100 °C, which is much higher than $A_f$, the decrease (~5%) is less pronounced. Higher test temperatures stabilize the austenite phase and therefore larger applied stresses

are required to initiate the forward transformation. The larger applied stresses are expected to reduce multiple variant formation and interaction, thus leading to reduced defect generation and hence reduced residual internal stress fields that would assist formation in subsequent cycles [1,15]. Without the influence of the internal stress fields, the critical stress is more stable at higher temperatures so they exhibit the smaller deviations with cycling. Unrecoverable deformation results from the residual martensite and slip in austenite and martensite domains. Internal stress fields are oriented favorably to accommodate the externally applied stress due to repeated cycling. As a result, more deformation is recovered with cycling and residual strain decreases from cycle to cycle.

The results for the [0 0 1] and [1 1 5] single crystals indicate a high degree of pseudoelastic recovery in compression but it is negligible under tension at 50 and 75 °C (Fig. 7). Since the stress levels are similar, the results point to the varying degrees of internal versus external stress-induced martensite variants in compression versus tension cases. Internal stress fields attributed to the second phase can resist or assist the nucleation of martensite variants. At temperatures closer to $A_f$, the austenite is less stable so internal stress fields are more effective. Internal stress fields appear to accommodate variants induced under compression and elastic energy storage proceeds uninhibited. Therefore, the stored elastic energy drives the reverse transformation to completion. In the tensile case, the internal stress fields compromise the elastic energy storage, and thus the reverse transformation is retarded and recovery must be completed via the SME. When the internal and external stress-induced variant interaction is decreased at higher test temperatures where a favorable single variant forms, pseudoelastic recovery is observed for both stress states. Elastic energy storage is also affected by the volumetric strain [7]. The volumetric contribution will be positive in tension and negative in compression as the normal dilatation is always positive. Consequently, the strain energy in tension is greater than in compression facilitating the transformation in tension while promoting plastic accommodation at the austenite–martensite interfaces. Plastic accommodation dissipates stored elastic energy. As a result, upon unloading, the driving force for the reverse transformation is compromised thus stabilizing the martensite, and minimal pseudoelastic recovery is observed. In compression, we expect minimal plastic deformation attributed to the volumetric strain and hence we observe a pseudoelastic response over a broad range of temperatures.

A clear tension–compression asymmetry of the maximum transformation strains and the stress hysteresis exists in the two-phase CoNi33Al27 single crystals (Figs. 8 and 10). The larger transformation strains measured under tension compared to compression agree with theoretical predictions. Although transformation strains as large as 6.2% are observed in tension for the [0 0 1] orientation, the non-transforming $\gamma$ phase prohibits the achievement of theoretical strains. The large volume fraction of this secondary phase limits the transformation strains by creating a barrier to transformation fronts and reducing the volume that can undergo phase change. Enhanced dislocation activity in these domains, particularly at the martensite–secondary phase interfaces, has been confirmed with TEM (Fig. 3(a)). Additionally, the external stress, which was limited to approximately 500 MPa to avoid fracture, does not allow the large detwinning strains to be attained. Meanwhile under compression, noticeably higher stresses are obtained that allow the maximum compressive transformation strains to exceed the theoretical CVP predictions, which suggests detwinning occurs in compression. Note that the theory does not consider the internally stressed configuration of the lattice, which could cause the deviation from the theoretical values. However, the non-linear unloading curves in Fig. 8(b), (d), and (e) strongly support that detwinning is likely achieved in compression.

The stress hysteresis growth with increasing applied strain is due to dislocation emission at transformation interfaces as well as to dislocations inherited from the severe plastic deformation of the second phase. Relaxation of coherent stresses at the advancing austenite–martensite interphase boundary, resulting from dislocation emission, causes stored elastic strain energy dissipation. Increasing the strain from 2% to 6% produces more severe plastic relaxation of coherent stresses at interphase boundaries concomitant with the transformation strain increase. Therefore, the contribution of the stored elastic strain energy to the reverse transformation is reduced and the hysteresis increases. In addition, increased plastic deformation of the second phase occurs as the applied strain is increased and the resulting dislocations can be inherited by martensite as it impinges upon the second phase (Fig. 3(a)). Considering Eq. (4), more intense plastic relaxation of martensite coherency strains would cause $\alpha$ to approach 0. As a result, the interaction energy term ($H^{nm}$) would increase as explained earlier and this causes the hysteresis increase for higher strains. The presence of dislocations remaining after the forward transformation enhances the frictional resistance to the reverse transformation. Recall that this increases the $F^C$ term in Eq. (4), thus creating another source of magnified hysteresis growth. The stress hysteresis is smaller for the tensile case, and the difference is noticeably larger for the nominally [1 2 3] crystals. We note that the tension compression asymmetry of the stress hysteresis is greatest for 6%. The [1 2 3] orientation is more favorably oriented for slip deformation and this is evidenced by the unrecoverable strain in Fig. 8(c) and (d). The intergranular constraint for the [1 2 3]N multicrystals promotes dissipation via frictional resistance, variant interaction, and dislocation emission. The large defect generation coupled with frictional dissipation leads to enormous stress hysteresis growth for the [1 2 3]N multicrystals under compression and tension. Furthermore, as a result of the large hysteresis growth under compression, the

[1 2 3] orientation displays the largest tension–compression asymmetry of the stress hysteresis (144 MPa) at 6% applied strain (see Fig. 10). The difference is large because CVP strains are exceeded in compression, which enhances frictional dissipation and stored elastic energy relaxation, and this observation lends further support that detwinning is achieved in compression.

The trends in thermal hysteresis growth (Fig. 10) with increasing isostress for thermal cycling experiments and stress hysteresis growth with increasing isothermal test temperature for stress–strain experiments are now considered. First, we note that the experimentally observed lower slope of the critical stress versus temperature dependence in tension implies a higher thermal hysteresis (assuming $M_s - \sigma$, $A_s - \sigma$ lines are parallel), which is indeed the case. A lower slope would decrease the $d\Sigma_{cr}/dT$ contribution in Eq. (4), and the stress hysteresis would also increase. With that stated, we now explain the contrasting isostress and isothermal hysteresis trends. Energetic contributions are different depending on variant interactions, which we now explain. The critical stress for the isothermal stress–strain experiments is higher than the stress levels achieved for the isostress thermal cycling experiments. Therefore, we expect variants oriented preferentially to the external stress to form during isothermal strain cycling. The lower stresses in the isostress thermal cycling case allow for intermixing of self-accommodating, external stress-induced martensite, and internal stress-induced martensite (i.e., multiple variant interactions). These contrasts promote the opposite trends in the growth of the thermal and stress hysteresis. In addition, residual strain remains in tension for the isostress experiments on [0 0 1] single crystals that is absent in compression. This implies that frictional resistance due to the presence of dislocations or residual martensite will be more influential than for compression, in which full recovery is observed. For this class of alloys we previously reported a large volumetric strain (~4.5%) that also magnifies the temperature hysteresis in tension. Apparently, the large volumetric strain is most influential during multiple variant interactions during thermal cycling in tension; a compressive external stress counteracts its influence. Although the stress hysteresis for the isothermal stress–strain case is smaller in tension than compression, both stress states exhibit similar stress hysteresis growth and critical transformation stability with increasing strain except for the nominal [1 2 3] crystals. The similarities indicate that the decreased variant interactions for the pseudoelastic case minimize the influence of dissipative mechanisms compared to isostress temperature cycling. Since the CVP transformation strains are lower than tension and the stresses are higher, we attribute the increased stress hysteresis in compression to increased frictional dissipation due to elastic deformation of martensite and the occurrence of detwinning.

The stress drop after $\sigma_{cr}$ in tension that is not observed in compression indicates differing transformation mechanisms at the onset of the transformation. The stress drop is indicative of a barrier to phase boundary motion as the martensite variants traverse across the specimens [17,18]. The barrier stress illustrates that a higher stress is required to nucleate martensite and initiate martensite reorientation than is necessary to propagate the transformation throughout the material. The reason for the noticeable absence of the barrier stress in compression is unclear and we consider it with regards to the volumetric strain. In tension, the strain energy will be higher due to the dilatational strain, and as the transformation progresses the strain energy is relaxed. Consequently a higher stress is needed to initiate the transformation than to sustain it in tension. The fact that this high stress is not achieved for the thermal cycling experiments supports our rationale for the larger thermal hysteresis in tension. Since the applied stresses are low in tension, the barrier stress is not exceeded. Dissipation due to multiple variant interaction is enhanced compared to compression, and tension displays a larger thermal hysteresis. The lack of a barrier stress in compression suggests this dissipative mechanism is minimized in compression and thus the thermal hysteresis is smaller.

It is known that during the low-cycle fatigue of SMAs, the critical transformation stress level decreases, the transformation stress–strain slope increases, and the dissipated hysteresis energy decreases [1]. A notable finding with CoNiAl is that the residual transformation strains decreased with cycling (Fig. 6(b)) near $A_f$. As the recovery increases, the transformation stress is relatively stable compared to polycrystalline CoNiAl [1]. Clearly, the critical stress even higher above $A_f$ is stable as illustrated in Fig. 5 at 100 °C. The stability of the critical stress is indicative of minimal plastic deformation of the austenite matrix as this would cause hardening behavior leading to an increase in the critical stress. Even though residual martensite exists, which typically lowers the critical stress for subsequent cycles, the critical stress remains stable. This apparent resilience against degradation in isothermal stress–strain cycling deserves further study and increases the potential utility of this class of materials.

Now we briefly summarize the influence of the intergranular constraint. The highest magnitude of and increase in critical (transformation) stress is for the multicrystals and polycrystals due to the intergranular constraint which facilitates the need for higher external stress to overcome misorientation effects as the temperature is raised. Polycrystals and multicrystals with nominal [1 2 3] orientation exhibit the largest transformation stress hysteresis, which is attributed to internal stresses at grain boundaries. The second phase most likely nucleates at grain boundaries. As a result, we expect the second-phase microstructure (i.e., size and interparticle separation) near grain boundaries to differ from that within the grain for the multicrystals and polycrystals. The resulting heterogeneous precipitate microstructure induces highly localized internal stress fields. Therefore, the interactions of internal versus external stress-induced martensite variants are enhanced, and since the second phase enhances dislocation generation

and martensite impingement (discussed previously), the hysteresis is larger than that of the single crystals. The obvious differences in stress hysteresis evolution, cyclic stability, and critical stress magnitudes clearly show the need for texture for this class of alloys.

## 6. Conclusions

1. Large transformation strains under tension (6.2%) and under compression (4.1%) were found for the [0 0 1] orientation. Although the $\gamma$ phase enhanced the ductility, it also limited the transformation strains and generated defects. These results are consistent with theoretical values outlined based on phenomenological theory of martensitic transformation.
2. The volumetric strain associated with the transformation altered the driving force for the transformation so as to assist under tension and resist under compression. This resulted in a modified slope of the well-known Clausius–Clapeyron relation. The volumetric strain had a drastic dissipative effect under tension at 50 °C which resulted in loss of pseudoelastic response. This effect is diminished under compression allowing for complete pseudoelastic recovery.
3. An equation for stress hysteresis is derived based on a complementary energy description accounting for interaction of martensite variants and dissipation due to plastic deformation at the austenite–martensite interfaces. The stress hysteresis increases with increased frictional resistance and increased variant interaction. The secondary phase deforms plastically, and in turn influences the hysteresis and transformation stress levels.
4. The prevailing outcome of the work is that these alloys undergo a large tensile volumetric strain, larger transformation strains in tension compared to compression, and higher transformation strains near the [0 0 1] orientation. The results point out to the need for texturing these materials such that the straining occurs preferentially near the [0 0 1] direction to achieve high transformation strains. Moreover, the available slip systems near the [0 0 1] orientation are limited and this increases the propensity for full recoverability.
5. The parent phase exhibits much less severe dislocation activity compared to the second phase. Cyclic recoverability is enhanced in these alloys or remains constant because plastic deformation occurs mainly in the second phase. The critical stress changed by approximately 18% at 50 °C for all orientations under both loading directions. At 100 °C the [0 0 1] and [1 1 5] orientations displayed stable critical stress levels.

## Acknowledgements

The work was supported by grants CMS-0428428, the National Science Foundation, Division of Civil and Mechanical Systems, and Deutsche Forschungsgemeinschaft (German portion of the work).

## References

[1] Efstathiou C, Sehitoglu H, Wagoner Johnson AJ, Hamilton RF, Maier HJ, Chumlyakov Y. Scripta Mater 2004;51:979–85.
[2] Karaca HE, Karaman I, Chumlyakov YI, Lagoudas DC, Zhang X. Scripta Mater 2004;51:261–6.
[3] Oikawa K, Omori T, Sutou Y, Kainum R, Ishida K. J Phys IV France 2003;112:1017–20.
[4] Oikawa K, Wulff L, Iijima T, Gejima F, Ohmori T, Fujita A, et al. Appl Phys Lett 2001;79:3290–2.
[5] Ishida K, Kainuma R, Ohtani H, Nishizawa T. In: Giamei AF, Inoue K, Mishima Y, editors. Mechanical properties and phase transformations of multiphase intermetallic alloys. Warrendale, PA: TMS; 1995. p. 77–90.
[6] Tanaka Y, Ohmori T, Oikawa K, Kainuma R, Ishida K. Mater Trans JIM 2004;45:427–30.
[7] Hamilton RF, Sehitoglu H, Efstathiou C, Maier HJ, Chumlyakov Y, Zhang XY. Scripta Mater 2005;53:131–6.
[8] Ishida K, Kainuma R, Ueno N, Nishizawa T. Metall Trans A 1991;22 A:441–6.
[9] Gall K, Sehitoglu H, Chumlyakov YI, Kireeva IV. Acta Mater 1999;47:1203–17.
[10] Orgeas L, Favier D. Acta Mater 1998;46:5579–91.
[11] Gall K, Sehitoglu H. Int J Plast 1999;15:69–92.
[12] Patoor E, Eberhardt A, Berveiller M. Pitman Res Notes Math Ser 1993;296:38.
[13] Niclaeys C, Ben Zineb T, Arbab-Chirani S, Patoor E. Int J Plast 2002;18:1619–47.
[14] Siredey N, Patoor E, Berveiller M, Eberhardt A. Int J Sol Struct 1999;36:4289–315.
[15] Hamilton RF, Sehitoglu H, Chumlyakov Y, Maier HJ. Acta Mater 2004;52:3383–402.
[16] Kainuma R, Ise M, Jia CC, Ohatani H, Ishida K. Intermetallics 1996;4:S151–8.
[17] Liu L, Xie Z, Van Humbeek J, Delay L. Scripta Mater 1999;41:1273–81.
[18] Liu L, Xie Z, Van Humbeek J, Delay L. Acta Mater 1998;46:4325–4338.